

# Enhanced magnetocaloric effect in frustrated magnets

M. E. Zhitomirsky

European Synchrotron Radiation Facility, BP-220, F-38043 Grenoble, France

SPSMS, Département de Recherche Fondamentale sur la Matière Condensée, CEA, F-38054 Grenoble, France\*

(Dated: October 26, 2018)

The magnetothermodynamics of strongly frustrated classical Heisenberg antiferromagnets on kagome, garnet, and pyrochlore lattices is examined. The field induced adiabatic temperature change  $(\partial T/\partial H)_S$  is significantly larger for such systems compared to ordinary non-frustrated magnets and also exceeds the cooling rate of an ideal paramagnet in a wide range of fields. An enhancement of the magnetocaloric effect is related to presence of a macroscopic number of soft modes in frustrated magnets below the saturation field. Theoretical predictions are confirmed with extensive Monte Carlo simulations.

PACS numbers: 75.30.Sg, 75.10.Hk, 75.50.Ee

## I. INTRODUCTION

The magnetocaloric effect consists in heating or cooling of matter in response to variations of external magnetic field. The technique of adiabatic demagnetization based on the magnetocaloric effect has been successfully utilized over the years to reach temperatures in a sub-Kelvin range.<sup>1</sup> Because of its technological simplicity and independence of gravity the magnetic cooling steadily attracts attention as a rival to the dilution refrigerators, especially in satellite applications.<sup>2,3,4</sup> Recent experimental studies of the magnetocaloric effect in specially designed materials have revealed the potential applicability of the magnetic cooling technique for room temperature refrigeration as well.<sup>5,6,7</sup>

Paramagnetic salts, which are standard refrigerant materials for the low-temperature magnetic cooling, contain dilute systems of magnetic dipoles. The entropy of an ideal paramagnet depends on magnetic field  $H$  and temperature  $T$  via  $H/T$ . Therefore, during adiabatic demagnetization, temperature of a paramagnet decreases *linearly* with a field:  $T/H = \text{const}$ . The higher the density of the magnetic moments and their spin number, the greater the cooling power of a refrigerant is. With increased density of spins, however, the strength of residual interactions between magnetic dipoles grows and leads to an ordering or a spin glass transition. The transition temperature  $T_c$ , which is roughly given by a strength of magnetic interactions, limits the lowest temperatures achievable with paramagnetic salts. Even above  $T_c$  the cooling becomes less efficient due to a reduced entropy, and the adiabatic temperature change is *slower* than in an ideal paramagnet. The cooling rate  $(\partial T/\partial H)_S$  of a salt does not, therefore, exceed the corresponding rate of a paramagnet:  $(\partial T/\partial H)_S^{\text{para}} = T/H$ .

The experimental and theoretical studies over the past decade have established a new distinct class of magnetic materials called geometrically frustrated magnets.<sup>8,9,10</sup> Magnetic ions in these systems form special types of lattices, Fig. 1. Despite interaction between neighboring spins, strongly frustrated magnets remain disordered and possess finite entropy at temperatures well below the

Curie-Weiss constant. This property suggests frustrated magnets as prospective candidates for use in the adiabatic demagnetization refrigerators. In fact, gadolinium gallium garnet  $\text{Gd}_3\text{Ga}_5\text{O}_{12}$  (GGG) has long been known as a suitable refrigerant material.<sup>11</sup> Recently, GGG with its unique phase diagram in magnetic field attracted a lot of interest from the point of view of geometric magnetic frustration on a garnet lattice.<sup>12</sup> In the present work we demonstrate a close relation between an enhanced magnetocaloric effect and strong geometric frustration. In particular,  $(\partial T/\partial H)_S$  in a frustrated magnet can exceed the cooling rate of an ideal paramagnet by more than an order of magnitude.

Specifically, we study an unusual magnetothermodynamics of classical Heisenberg antiferromagnets on several frustrated lattices. The choice of classical models is motivated by large values of spins of the magnetic ions in frustrated magnets:  $\text{Cr}^{3+}$  ( $S = 3/2$ ),  $\text{Fe}^{3+}$  ( $S = 5/2$ ), and  $\text{Gd}^{3+}$  ( $S = 7/2$ ).<sup>8,9</sup> The studied frustrated structures include two- (2D) and three-dimensional (3D) networks of corner-sharing triangles known as a kagome, Fig. 1a, and a garnet lattice, Fig. 1b, and a 3D network of corner-sharing tetrahedra of a pyrochlore lattice, Fig. 1c. In all three cases the magnetic Hamiltonian includes exchange interaction of strength  $J$  between the nearest-neighbor classical spins of unit length and the Zeeman energy:

$$\hat{\mathcal{H}} = J \sum_{\langle ij \rangle} \mathbf{S}_i \cdot \mathbf{S}_j - \mathbf{H} \cdot \sum_i \mathbf{S}_i. \quad (1)$$

The main distinction of strongly frustrated magnets is a large, macroscopic degeneracy of their classical ground states in zero magnetic field. It arises due to a so called under-constraint: condition of the minimal energy for every elementary frustrated unit, triangle or tetrahedron, is not sufficient to fix all microscopic degrees of freedom.<sup>8,10</sup> In applied magnetic field the macroscopic degeneracy persists up to the saturation field  $H_{\text{sat}}$ , which is  $H_{\text{sat}} = 6J$  for kagome and garnet antiferromagnets and  $H_{\text{sat}} = 8J$  for a pyrochlore antiferromagnet.<sup>13,14</sup> At zero temperature frustrated magnets loose their degeneracy and become completely polarized above  $H_{\text{sat}}$ . Transformation from the unique ground state at  $H > H_{\text{sat}}$  to

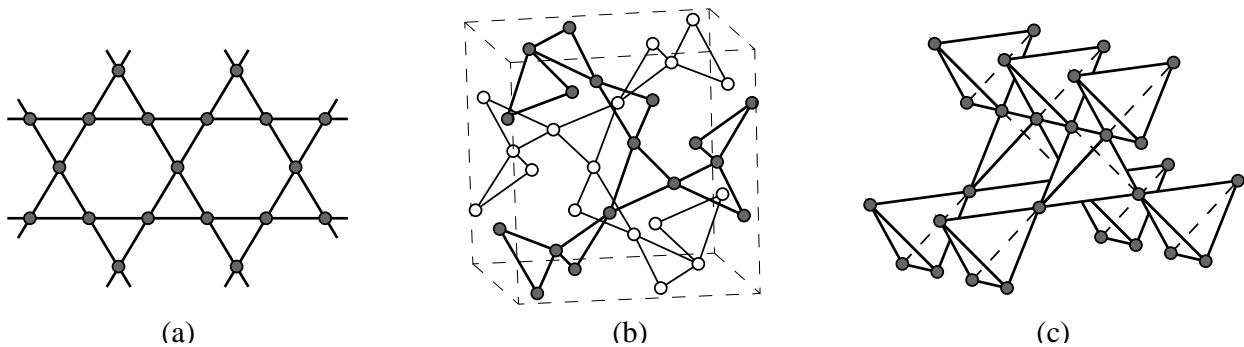


FIG. 1: Magnetic systems with strong frustration: (a) kagome lattice, (b) garnet lattice, and (c) pyrochlore lattice.

an infinitely degenerate ground state at  $H < H_{\text{sat}}$  is accompanied by condensation of a macroscopic number of zero-energy modes.<sup>14,15</sup> This should be contrasted with the behavior of non- or weakly-frustrated magnets, where the antiferromagnetic state below  $H_{\text{sat}}$  is described by a certain wave-vector and, therefore, the phase transition at  $H = H_{\text{sat}}$  corresponds to condensation of one or a few zero-energy modes. In the vicinity of  $H_{\text{sat}}$  the thermodynamic properties of a strongly frustrated magnet are, therefore, controlled by flat branches of excitations with vanishing energy at  $H = H_{\text{sat}}$ .

The following theoretical analysis is divided into two parts. The next section gives a general thermodynamic description of magnets with a macroscopic number of soft excitations. We also calculate the number of such modes for the three frustrated spin models. The subsequent section describes Monte Carlo results for various thermodynamic quantities of frustrated models and also simulations of the adiabatic demagnetization process for a few frustrated and non-frustrated magnets. These are followed by discussion of suitable magnetic materials, which can exhibit the predicted behavior.

## II. THEORY

Our aim in this section is to understand the effect of soft modes on a cooling rate of a strongly frustrated magnet under adiabatic demagnetization. The cooling rate is related to isothermal characteristics by

$$\left(\frac{\partial T}{\partial H}\right)_S = -T \frac{(\partial S / \partial H)_T}{C}, \quad (2)$$

where  $C$  is the specific heat in a constant magnetic field. We shall also use the normalized rate dividing (2) by the cooling rate of an ideal paramagnet  $(\partial T / \partial H)_S^{\text{para}} = T/H$ . Values  $(\partial T / \partial H)_S^{\text{norm}} > 1$  indicate that a magnet cools down faster than a paramagnet in a certain range of fields and temperatures. The cooling rate is enhanced for systems with large negative values of  $(\partial S / \partial H)_T$ .

### A. Magnetothermodynamics

A classical magnet on an  $N$ -site lattice has  $2N$  degrees of freedom in total with two modes per spin. In the saturated phase above  $H_{\text{sat}}$  all  $2N$  magnetic excitations are gapped. In the harmonic approximation the excitation energies of non-frustrated magnets are given by

$$\omega(\mathbf{k}) = H - H_{\text{sat}} + \varepsilon(\mathbf{k}), \quad (3)$$

where  $\varepsilon(\mathbf{k})$  is nonnegative and vanishes at one or a few points in the Brillouin zone. Non-Bravais lattices have several modes for every wave-vector  $\mathbf{k}$  and below we imply summation over all such branches. At low temperatures anharmonic effects are small, which allows to find explicitly the fluctuation contributions to various physical quantities. In particular, the specific heat per one spin is  $C = 1$  ( $k_B \equiv 1$ ) and

$$\left(\frac{\partial S}{\partial H}\right)_T = -\frac{1}{2} \sum_{\mathbf{k}} \frac{1}{H - H_{\text{sat}} + \varepsilon(\mathbf{k})}. \quad (4)$$

Since  $\varepsilon(\mathbf{k}) \sim k^2$  near its zeroes,  $(\partial S / \partial H)_T$  at  $H = H_{\text{sat}}$  is a  $T$ -independent constant in 3D and has a weak logarithmic singularity in 2D.

The excitation spectra of strongly frustrated magnets in the saturated phase are special in that  $\varepsilon(\mathbf{k}) \equiv 0$  in the whole Brillouin zone for several flat branches of excitations. We denote the number of such modes as  $N_4$ ,  $N_2$  being the number of ordinary dispersive modes (3) and  $N_2 + N_4 = 2N$ . As field approaches  $H_{\text{sat}}$ , the contribution from soft dispersionless excitations grows and the harmonic approximation fails. To study the effect of soft modes one needs to consider an anharmonic energy functional of the type:

$$E = \sum_{\mathbf{k}} (H - H_{\text{sat}}) |y_{\mathbf{k}}|^2 + \sum_{\mathbf{k}, \mathbf{p}, \mathbf{q}} V_{\mathbf{k}\mathbf{p}}^{\mathbf{q}} y_{\mathbf{k}+\mathbf{q}}^* y_{\mathbf{p}-\mathbf{q}}^* y_{\mathbf{p}} y_{\mathbf{k}}, \quad (5)$$

where  $y_{\mathbf{k}}$ 's denote collective coordinates of soft modes and  $V_{\mathbf{k}\mathbf{p}}^{\mathbf{q}} \sim J$  are nonnegative interaction constants. Cubic terms vanish in the expansion by a spin-rotational symmetry. Also, an interaction between soft and the harmonic modes can be neglected at low temperatures. The

above energy functional determines scaling of the corresponding contribution to the free energy:

$$F_4 = -\frac{N_4}{4} T \ln T - T f \left( \frac{H - H_{\text{sat}}}{\sqrt{T}} \right). \quad (6)$$

The function  $f(u)$  has the following asymptotes:  $f(u) \approx f(0) + uf'(0)$  with  $f(0) > 0$  and  $f'(0) < 0$  as  $u \rightarrow 0$ , and  $f(u) \approx -(N_4/2) \ln u$  as  $u \rightarrow \infty$ .

It follows from Eq. (6) that the specific heat and the magnetic susceptibility depend on magnetic field and temperature only via combination  $(H - H_{\text{sat}})/\sqrt{T}$ .<sup>14</sup> In particular, the specific heat per one spin reaches a universal fractional value at  $H = H_{\text{sat}}$ :  $C = (\frac{1}{2}N_2 + \frac{1}{4}N_4)/N = 1 - N_4/(4N)$ . For the magnetocaloric effect, Eq. (6) gives at  $H = H_{\text{sat}}$ :

$$\left( \frac{\partial S}{\partial H} \right)_T \propto -\frac{N_4}{\sqrt{T}}, \quad (7)$$

which significantly exceeds the contribution of dispersive modes Eq. (4). Thus, condensation of a macroscopic number of zero-energy modes at the saturation field greatly enhances the magnetocaloric effect in strongly frustrated magnets at low temperatures. An important characteristics of a magnet is, then, the number of soft modes  $N_4$ .

## B. Soft modes

### 1. Kagome antiferromagnet

In order to find the number of soft modes we perform classical spin-wave calculations in the saturated collinear state. A primitive unit cell of a kagome lattice contains one triangular plaquette. The corresponding Bravais lattice has  $N/3$  states. Expanding spin components along the field in small transverse deviations we obtain a classical spin-wave Hamiltonian to a desired order. In the harmonic approximation two transverse polarizations for the spin excitations are independent. As a result, the spectrum consists of three double-degenerate modes:

$$\begin{aligned} \omega_1(\mathbf{k}) &= H - 6J, \\ \omega_{2,3}(\mathbf{k}) &= H - 3J \pm J\sqrt{3(1 + 2\gamma_{\mathbf{k}})}, \end{aligned} \quad (8)$$

where  $\gamma_{\mathbf{k}} = \frac{1}{3}(\cos k_x + 2 \cos \frac{1}{2}k_x \cos \frac{\sqrt{3}}{2}k_y)$ . The total number of soft quartic modes at  $H_{\text{sat}} = 6J$  is, therefore,  $N_4^{\text{kag}} = 2N/3$ . This is exactly twice the number of hexagon voids on a kagome lattice. The correspondence between such voids and soft modes has first been found for a kagome antiferromagnet in zero field<sup>16</sup> and was, later, extended to finite magnetic fields.<sup>14</sup> Local soft modes in the collinear state at  $H = H_{\text{sat}}$  consist in alternate tilting of spins around elementary hexagons in two different directions perpendicular to the field. The

geometric picture of local soft modes can be straightforwardly generalized for a classical spin model on a checkerboard lattice, which is the other planar frustrated lattice with voids around empty squares.<sup>15</sup> The checkerboard antiferromagnet has  $N$  local zero-energy modes at  $H_{\text{sat}} = 8J$ .

### 2. Pyrochlore antiferromagnet

The spin-wave calculations for a pyrochlore antiferromagnet yield four double-degenerate modes defined in the Brillouin zone of a face-centered cubic (fcc) lattice, which has  $N/4$  states:

$$\begin{aligned} \omega_{1,2}(\mathbf{k}) &= H - 8J, \\ \omega_{3,4}(\mathbf{k}) &= H - 4J \pm 2J\sqrt{1 + 3\nu_{\mathbf{k}}} \end{aligned} \quad (9)$$

with  $\nu_{\mathbf{k}} = \frac{1}{6}(\cos k_x + \cos k_y + 4 \cos k_z \cos \frac{1}{2}k_x \cos \frac{1}{2}k_y)$ . The total number of zero modes in a pyrochlore antiferromagnet at the saturation field is  $N_4^{\text{pyr}} = N$ , *i.e.* the same

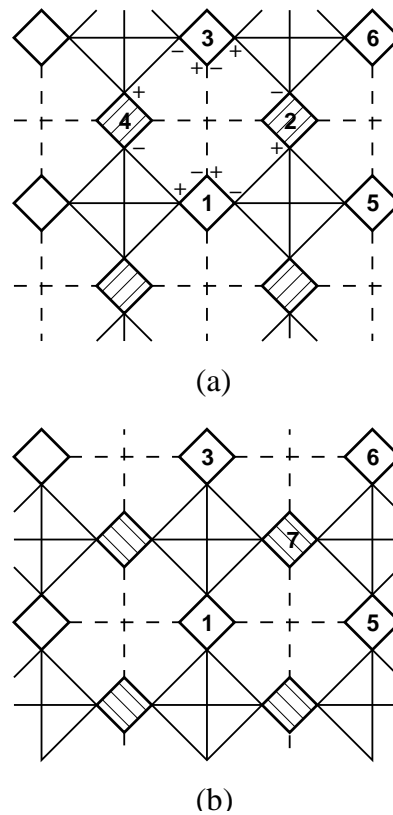


FIG. 2: Two projections of a pyrochlore lattice on a (001) plane. Small, light and dashed, squares represent one type of tetrahedra; big squares with crosses correspond to the other type of tetrahedra. Small light tetrahedra belong to the same (001) plane of an fcc lattice. Small dashed tetrahedra lie in an adjacent plane: (a) below and (b) above. Soft spin modes on hexagon loops  $l_{123}$  and  $l_{134}$  are shown with +’s and -’s on the top panel.

as for the checker-board model. The geometric interpretation of these modes becomes, however, more complicated. A dispersionless soft mode can still be attributed to a local perturbation in the collinear structure: alternate tilting of spins around a closed line, which shares two vertices with each crossed tetrahedron. The shortest such loop on a pyrochlore lattice is a hexagon. Simple counting yields  $N$  hexagons for an  $N$ -site pyrochlore lattice. If a one-to-one correspondence between the soft modes and the hexagons holds, then the above number would imply  $2N$  soft modes, which is twice more than the spin-wave prediction. The contradiction is resolved in favor of the spin-wave result by establishing that some of the hexagon loops on a pyrochlore lattice are linearly dependent with total  $N/2$  linear relations. This brings the number of independent hexagon spin-loops (modes) to  $N/2$  in agreement with the spin-wave expansion. Below, we briefly sketch a proof of the above statement.

A pyrochlore lattice, Fig. 1c, is formed with two types of tetrahedra. To simplify geometric representation we draw a pyrochlore structure as an fcc lattice constructed from one type of tetrahedra. A cut through such a lattice along (001) plane is shown in Fig. 2. Hexagons in Fig. 2 correspond to closed loops which include two tetrahedra in one layer and one tetrahedron in an adjacent layer. Soft spin modes on two such loops are shown in Fig. 2 with pluses and minuses, which indicate alternate tilting of spins from the field direction. The first type of a linear relation between spin-loops appears for a block formed by four tetrahedra numbered 1–4 in Fig. 2a. A superposition of the local soft modes corresponding to hexagon loops  $l_{123}$  and  $l_{134}$  leaves two inner spins unmoved and tilts only outer spins around the block perimeter. The same eight-spin mode is obtained by a superposition of spin-

loops  $l_{124}$  and  $l_{234}$ . Thus, every such block of four tetrahedra provides one linear relation between four loops. This reduces the number of independent spin-loops by the number of such blocks  $N/4$ . The second type of a linear relation corresponds to a block of six tetrahedra: four in one layer, 1, 3, 5, and 6, and two in adjacent layers, 2 and 7, Figs. 2a,b. A superposition of spin-loops  $l_{123}$  and  $l_{256}$  corresponds to the same mode as a superposition of  $l_{157}$  and  $l_{367}$ . Counting all such blocks brings additional  $N/4$  linear relations. This makes in total  $N/2$  linear relations between hexagonal spin-loops and, hence,  $N_4^{\text{pyr}} = 2(N - N/2) = N$  soft modes for a pyrochlore antiferromagnet at the saturation field. Composite low-energy excitations on six-spin loops, which are similar to the above soft modes, have been recently observed in neutron scattering studies of pyrochlore antiferromagnet  $\text{ZnCr}_2\text{O}_4$  in zero field.<sup>17</sup>

### 3. Garnet antiferromagnet

The structure of a garnet lattice is by far the most complicated among frustrated lattices. In GGG the magnetic  $\text{Gd}^{3+}$  ions form two interpenetrating triangular sublattices with 24 atoms per a cubic unit cell. Exchange interaction couples each spin with its nearest-neighbors from the same sublattice. Spins on two different sublattices interact only via weaker dipolar forces. In the present study we focus on the behavior of an exchange model and, therefore, consider only one sublattice of corner-sharing triangles with 12 spins per a unit cell represented, e.g., by dark circles in Fig. 1b. The nearest-neighbor exchange Hamiltonian on a garnet lattice can be written as

$$\begin{aligned} \mathcal{H} = J \sum_i & \left[ \mathbf{S}_{1i} \cdot (\mathbf{S}_{2i} + \mathbf{S}_{3i} + \mathbf{S}_{4i+x} + \mathbf{S}_{5i+x}) + \mathbf{S}_{2i} \cdot (\mathbf{S}_{3i} + \mathbf{S}_{6i+y} + \mathbf{S}_{7i+y}) + \mathbf{S}_{3i} \cdot (\mathbf{S}_{8i+z} + \mathbf{S}_{9i+z}) \right. \\ & + \mathbf{S}_{4i} \cdot (\mathbf{S}_{5i} + \mathbf{S}_{8i+z} + \mathbf{S}_{10i+z}) + \mathbf{S}_{5i} \cdot (\mathbf{S}_{6i-x} + \mathbf{S}_{11i}) + \mathbf{S}_{6i} \cdot (\mathbf{S}_{7i} + \mathbf{S}_{11i+x}) + \mathbf{S}_{7i} \cdot (\mathbf{S}_{9i-y} + \mathbf{S}_{12i}) \\ & \left. + \mathbf{S}_{8i} \cdot (\mathbf{S}_{9i} + \mathbf{S}_{10i}) + \mathbf{S}_{9i} \cdot \mathbf{S}_{12i+y} + \mathbf{S}_{10i} \cdot (\mathbf{S}_{11i} + \mathbf{S}_{12i}) + \mathbf{S}_{11i} \cdot \mathbf{S}_{12i} \right] + \mathcal{H}_{\text{Zeeman}}, \end{aligned} \quad (10)$$

where the first spin index  $j = 1-12$  is the site number in a unit cell and the second spin index  $i$  is the cell number on a cubic lattice;  $i \pm x, \dots$  being adjacent cells along three orthogonal directions.

After Fourier transformation the spin-wave energies are given by eigenvalues of a  $12 \times 12$  matrix. The corresponding equation factorizes into a product of  $(\omega - H + 6J)^4$  and an eighth-order polynomial in  $\omega$ .<sup>18</sup> At  $H = 6J$  there are exactly four zero roots for an arbitrary value of the wave-vector. Zero eigenvalues determine  $N_4^{\text{gar}} = 2N/3$  soft modes at the saturation field, which is the same number as for a kagome antiferromag-

net. Thus, the term *hyper-kagome* used sometimes to refer to a garnet structure receives an extra justification. Geometric picture of soft modes in a hyper-kagome antiferromagnet is, however, much more complicated than in its planar counterpart. The shortest closed loop on a garnet lattice, which corresponds to an elementary soft mode, crosses ten triangles. At the same time each bond between a pair of nearest-neighbor spins participates in five such loops.<sup>19</sup> This should be contrasted with simple hexagon loops on a kagome lattice, where every bond is included in one loop only. The total number of ten-triangle loops for a garnet lattice is calculated to be  $N$ .

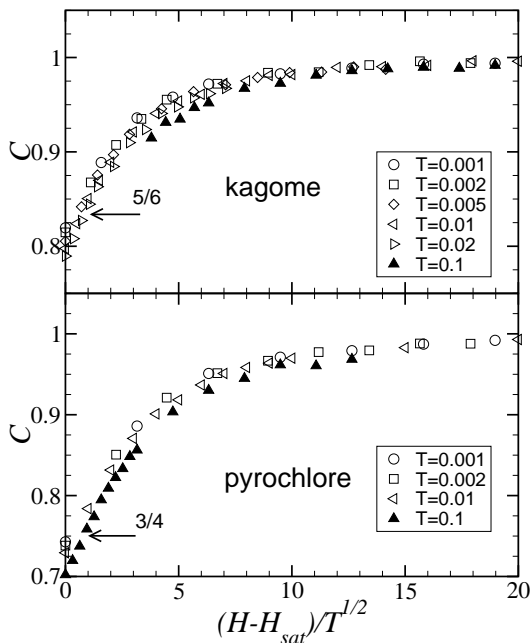


FIG. 3: Scaling behavior of the specific heat in the saturated phase for a kagome (top panel) and a pyrochlore (bottom panel) antiferromagnet. Different symbols correspond to field-scans performed at several fixed temperatures. Arrows indicate the limiting values of the specific heat per one site at the saturation field. Fields and temperatures are given in units of  $J$ .

A comparison with  $N/3$  soft modes for one transverse polarization found in the spin-wave analysis suggests that there are  $2N/3$  linear relations between closed loops for a garnet structure. An underlying geometric picture behind these relations remains to be clarified.

To conclude this section we note that a pyrochlore lattice is the most frustrated one among the above three structures, because it has the largest number of soft modes. The same is also true in zero magnetic field, where a classical Heisenberg pyrochlore lattice antiferromagnet remains disordered down to lowest temperatures,<sup>20</sup> whereas a classical kagome antiferromagnet develops a unique planar triatic order parameter.<sup>14,16</sup> As a result, a pyrochlore antiferromagnet should exhibit the fastest cooling rate under adiabatic demagnetization among frustrated magnets.

### III. MONTE CARLO SIMULATIONS

Monte Carlo (MC) simulations of the three spin models have been performed with the standard Metropolis algorithm. To improve statistics at low temperatures we introduce a maximum change  $\Delta S^z = 3T$  for a choice of a new spin direction in the local coordinate frame. In this way an acceptance rate for spin moves is kept at the level of 30%. (Other values  $\Delta S^z/T \sim 1-5$  will work as well.) MC simulations are done on finite clus-

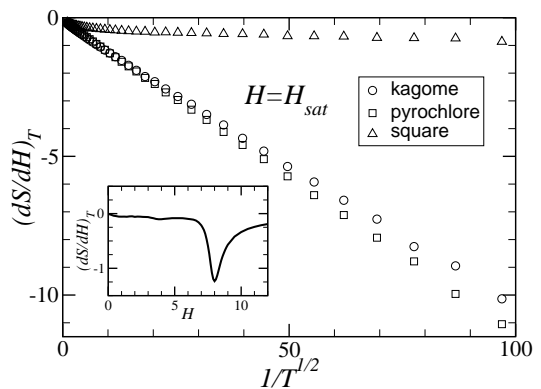


FIG. 4: Scaling behavior of  $(\partial S/\partial H)_T$  at  $H = H_{\text{sat}}$  in kagome and pyrochlore antiferromagnets. Inset shows the field dependence of  $(\partial S/\partial H)_T$  at  $T = 0.01J$  for a pyrochlore antiferromagnet. Fields and temperatures are given in units of  $J$ .

ters with periodic boundary conditions. Typical cluster sizes are  $N = 3 \times 18^2 = 972$  for a kagome lattice,  $N = 4 \times 6^3 = 864$  for a pyrochlore lattice, and  $N = 12 \times 5^3 = 1500$  for a garnet lattice. Comparison with smaller and larger clusters have been made to insure that finite-size corrections are small. Typical MC runs are carried with  $10^5$  MC steps per spin for equilibration followed by averaging over  $10^5$  measurements made in intervals of 5–10 MC steps. Statistical errors are estimated by performing several ( $\sim 5$ ) runs from different initial configurations. The errors for all presented data are small and do not exceed symbol sizes. The specific heat is calculated from the variance of the total energy:  $C = (\langle E^2 \rangle - \langle E \rangle^2)/T^2$ , while the magnetocaloric effect is expressed via a cumulant of the energy and the magnetization:  $(\partial S/\partial H)_T = (\langle EM \rangle - \langle E \rangle \langle M \rangle)/T$ .

We present in Fig. 3 the specific heat per one site of kagome and pyrochlore antiferromagnets plotted with respect to the scaling parameter  $u = (H - H_{\text{sat}})/\sqrt{T} > 0$ . The data have been collected during field-scans at fixed temperatures. Points from different scans, except of the highest temperature of  $T = 0.1J$ , fall on the same curve confirming the predicted scaling form. The specific heat at  $H = H_{\text{sat}}$  ( $u = 0$ ) reaches values which are close to the asymptotic results derived from the number of soft quartic modes:  $C = 5/6$  and  $C = 3/4$  for a kagome and a pyrochlore antiferromagnet, respectively. The magnetocaloric effect near saturation is presented in Fig. 4. The main plot shows temperature dependence of  $(\partial S/\partial H)_T$  exactly at the saturation field for kagome, pyrochlore and square lattice (576-site cluster) antiferromagnets. Numerical results for a garnet antiferromagnet are not included because at  $H > H_{\text{sat}}$  they virtually coincide with the data for a kagome antiferromagnet. Significant difference (Fig. 4) between the frustrated magnets on one side and a non-frustrated square lattice antiferromagnet on the other side confirms an enhancement of the magnetocaloric effect related to magnetic frustration. A range of magnetic fields in the vicinity of  $H_{\text{sat}}$ , where such an

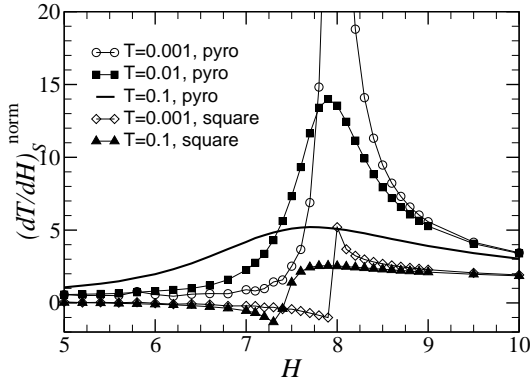


FIG. 5: Cooling rates of pyrochlore and square lattice antiferromagnets normalized to a cooling rate of an ideal paramagnet. Fields and temperatures are given in units of  $J$ .

enhancement occurs, is illustrated on the inset.

Direct comparison of the cooling rates of magnets with and without frustration is made in Fig. 5, where results for a pyrochlore and a square lattice antiferromagnet are plotted for several field scans. The two magnets have the same saturation field  $H_{\text{sat}} = 8J$ . For a pyrochlore antiferromagnet this field corresponds to a crossover from the nondegenerate saturated phase into a highly degenerate state below  $H_{\text{sat}}$ . The crossover is accompanied by a large increase in the adiabatic temperature variation, which exceeds the cooling rate of an ideal paramagnet by more than an order of magnitude. In contrast the spin model on a square lattice has a real transition near  $H_{\text{sat}}$  into a nondegenerate antiferromagnetic state with divergent correlation length. The cooling rate becomes negative below the transition, which means that a magnet heats up during demagnetization rather than cooling down. There is also no significant enhancement of the cooling rate above  $H_{\text{sat}}$  apart from a small narrow peak due to an anomaly in  $(\partial S/\partial H)_T$  at the transition.

Finally, a full adiabatic demagnetization process can be simulated with MC by measuring at fixed  $T$  and  $H$  isothermal characteristics  $C$  and  $(\partial S/\partial H)_T$  to find the cooling rate (2) and, then, choosing a new value of temperature according to  $\Delta T_{\text{ad}}/\Delta H = (\partial T/\partial H)_S$  for sufficiently small  $\Delta H$ . Adiabatic temperature changes for demagnetization from two starting temperatures  $T = J$  and  $T = 0.1J$  and the same initial field  $H = 9J$  are shown for garnet, pyrochlore, and cubic ( $N = 512$ ) antiferromagnets in Fig. 6. Since saturation fields for the three magnets are different, we use rescaled exchange constants  $J^* = 0.75J$  for a pyrochlore and  $J^* = 0.5J$  for a cubic antiferromagnet to set the common saturation field of  $H_{\text{sat}} = 6J$  in all three cases. During demagnetization the non-frustrated cubic antiferromagnet has the smallest relative temperature variation and starts to heat up below the transition into antiferromagnetically ordered state. The adiabatic temperature decrease for frustrated magnets is much larger with the largest effect exhibited by a pyrochlore antiferromagnet. Note, that tem-

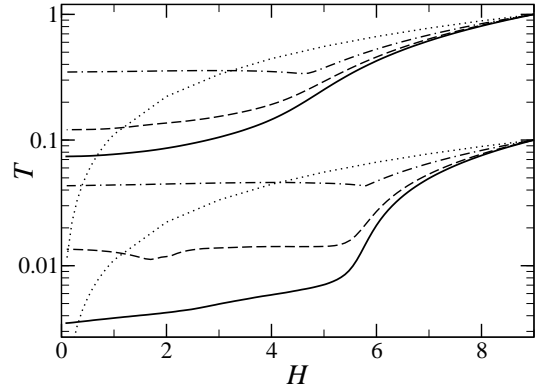


FIG. 6: Temperature variation during adiabatic demagnetization of a pyrochlore (full line), a garnet (dashed line), and a cubic (dot-dashed line) antiferromagnet. Dotted lines represent demagnetization of an ideal paramagnet ( $T/H = \text{const}$ ). Fields and temperatures are given in units of  $J$ .

perature of a pyrochlore antiferromagnet drops by more than ten times as field decreases from  $H_{\text{ini}} = 1.5H_{\text{sat}}$  to  $H_{\text{fin}} = 0.8H_{\text{sat}}$ . To achieve a similar cooling with a paramagnetic salt magnetic field has to be decreased at least by a factor of ten. The two distinctive features of the demagnetization of a pyrochlore antiferromagnet are (i) a persistent temperature decrease up to a zero field, though with a reduced cooling rate below  $H_{\text{sat}}$ , and (ii) an increase in the relative temperature variation as a starting temperature goes down, which is a consequence of the low-temperature singularity (7).

#### IV. DISCUSSION

The practical limitation on experimental observation of an enhanced magnetocaloric effect comes from a strength of the saturation field. At present, only frustrated magnets with exchange constants of the order of few Kelvin or less can be saturated with dc magnetic fields. The prime example is gadolinium gallium garnet with  $H_{\text{sat}} \simeq 1.7 \text{ T}$ ,<sup>12</sup> which is a popular refrigerant material in an applied experimental research on the magnetic cooling.<sup>4,11</sup> Quantitative comparison of the cooling rates of an ideal paramagnet and a Heisenberg garnet antiferromagnet is made in Fig. 6. Starting with the same temperature a garnet antiferromagnet cools down to much lower temperatures than a paramagnet in a wide range of magnetic fields. There are also two pyrochlore antiferromagnets  $\text{Gd}_2\text{Ti}_2\text{O}_7$  and  $\text{Gd}_2\text{Sn}_2\text{O}_7$ ,<sup>21,22,23</sup> which have saturation fields about 7 T. It is an interesting experimental challenge to observe the fast temperature decrease upon adiabatic demagnetization in these materials. Operation with relatively high magnetic fields makes rather questionable a technological application of the two gadolinium pyrochlores. The theoretical results suggest, though, a new direction for a search of suitable materials: a pyrochlore antiferromagnet with a factor of four smaller

exchange constant than in  $\text{Gd}_2\text{Ti}_2\text{O}_7$  would be a more efficient refrigerant than  $\text{Gd}_3\text{Ga}_5\text{O}_{12}$ , while operating in a similar range of fields and temperatures.

Real materials have, of course, more complicated magnetic interactions than just a nearest-neighbor exchange between classical spins. For example, in GGG a dipole-dipole interaction between neighboring spins amounts to 20–30% of the corresponding exchange energy.<sup>12</sup> Long-range dipolar interactions play also a significant role in the two pyrochlore compounds.<sup>21,22</sup> Influence of these and other extra perturbations on the magnetocaloric effect in frustrated magnets requires further theoretical analysis. Meantime, one can make several general remarks on the relative importance of various perturbations. The quantum effects omitted in the present study do not destroy the anomalous magnetothermodynamics near  $H_{\text{sat}}$ . Similar to their classical counterparts quantum antiferromagnets on the three frustrated lattices also have flat branches of excitations.<sup>15</sup> The anomaly (7) is,

nevertheless, affected by a weak dispersion ( $\sim J_{\text{disp}}$ ) of soft excitations induced, e.g., by a second-neighbor exchange or dipole-dipole interactions. The magnetocaloric effect will saturate below  $T^* \sim J_{\text{disp}}$  at  $(\partial S/\partial H)_T \sim 1/\sqrt{T^*}$ , which could be relatively large. Such a frustrated magnet can still be used, though less efficiently, as a refrigerant to reach temperatures below  $T^*$ . A further analysis of a destructive role of various perturbations should focus, therefore, on an induced dispersion in flat magnon branches.

## Acknowledgments

I am greatly indebted to T. M. Rice, who's questions have inspired this study. In the course of the work I benefited from fruitful discussions with A. I. Golov, C. L. Henley, A. Honecker, A. R. Muratov, and O. A. Petrenko.

---

\* permanent address.

- <sup>1</sup> O. V. Lounasmaa, *Experimental Principles and Methods Below 1K*, chapter 5 (Academic Press, London, 1974).
- <sup>2</sup> C. Hagmann, D. J. Benford, and P. L. Richards, *Cryogenics* **34**, 213 (1994); C. Hagmann and P. L. Richards, *ibid.* **35**, 303 (1995).
- <sup>3</sup> W. J. McRae, E. N. Smith, J. Beamish, J. M. Parpia, J. Low Temp. Phys. **121**, 809 (2000).
- <sup>4</sup> A. Kushino, Y. Aoki, N. Y. Yamasaki, T. Namiki, Y. Ishisaki, T. Matsuda, T. Ohashi, K. Mitsuda, and T. Yazawa, *J. Appl. Phys.* **90**, 5812 (2001).
- <sup>5</sup> V. K. Pecharsky and K. A. Gschneidner, *Phys. Rev. Lett.* **78**, 4494 (1997).
- <sup>6</sup> A. Giguère, M. Foldeaki, B. Ravi Gopal, R. Chahine, T. K. Bose, A. Frydman, and J. A. Barclay, *Phys. Rev. Lett.* **83**, 2262 (1999).
- <sup>7</sup> O. Tegus, E. Brück, K. H. J. Buschow, and F. R. de Boer, *Nature* **415**, 150 (2002).
- <sup>8</sup> A. P. Ramirez, *Annu. Rev. Mater. Sci.* **24**, 453 (1994); P. Schiffer and A. P. Ramirez, *Comments Cond. Mat. Phys.* **18**, 21 (1996).
- <sup>9</sup> J. E. Greedan, *J. Mater. Chem.* **11**, 37 (2001).
- <sup>10</sup> R. Moessner, *Can. J. Phys.* **79**, 1283 (2001).
- <sup>11</sup> J. A. Barclay and W. A. Steyert, *Cryogenics* **22**, 73 (1982); A. F. Lacaze, R. Beranger, G. Bon-Mardion, G. Claudet, and A. A. Lacaze, *ibid.* **23**, 427 (1983).
- <sup>12</sup> S. Hov, H. Bratsberg, and A. T. Skjeltorp, *J. Magn. Magn. Mater.* **15–18**, 455 (1980); P. Schiffer, A. P. Ramirez, D. A. Huse, and A. J. Valentino, *Phys. Rev. Lett.* **73**, 2500 (1994); O. A. Petrenko, C. Ritter, M. Yethiraj, and D. McK Paul, *Phys. Rev. Lett.* **80**, 4570 (1998); Y. K. Tsui, C. A. Burns, J. Snyder, and P. Schiffer, *Phys. Rev. Lett.* **82**, 3532 (1999); Y. K. Tsui, J. Snyder, and P. Schiffer, *Phys. Rev. B* **64**, 012412 (2001).
- <sup>13</sup> M. E. Zhitomirsky, A. Honecker, and O. A. Petrenko, *Phys. Rev. Lett.* **85**, 3269 (2000).
- <sup>14</sup> M. E. Zhitomirsky, *Phys. Rev. Lett.* **88**, 057204 (2002).
- <sup>15</sup> J. Schulenburg, A. Honecker, J. Schnack, J. Richter, and H.-J. Schmidt *Phys. Rev. Lett.* **88**, 167207 (2002).
- <sup>16</sup> J. T. Chalker, P. C. W. Holdsworth, and E. F. Shender, *Phys. Rev. Lett.* **68**, 855 (1992).
- <sup>17</sup> S.-H. Lee, C. Broholm, W. Ratcliff, G. Gasparovic, Q. Huang, T. H. Kim, and S.-W. Cheong, *Nature* **418**, 856 (2002).
- <sup>18</sup> we use the MATHEMATICA software for this calculation.
- <sup>19</sup> C. L. Henley and O. A. Petrenko, private communication.
- <sup>20</sup> R. Moessner and J. T. Chalker, *Phys. Rev. B* **58**, 12049 (1998).
- <sup>21</sup> N. P. Raju, M. Dion, M. J. P. Gingras, T. E. Mason, and J. E. Greedan, *Phys. Rev. B* **59**, 14489 (1999).
- <sup>22</sup> A. P. Ramirez, B. S. Shastry, A. Hayashi, J. J. Krajewski, D. A. Huse, and R. J. Cava, *Phys. Rev. Lett.* **89**, 067202 (2002).
- <sup>23</sup> V. Bondah-Jagalu and S. T. Bramwell, *Can. J. Phys.* **79**, 1381 (2001).